nature photonics

Article

https://doi.org/10.1038/s41566-025-01792-0

Quantum fusion of independent networks based on multi-user entanglement swapping

Received: 22 November 2023

Accepted: 1 October 2025

Published online: 4 November 2025

Check for updates

Yiwen Huang[1,5], Yilin Yang[1,5], Hao Li[1,5], Jiayu Wang[1], Jing Qiu[1], Zhantong Qi[1], Yuting Zhang[1], Yuanhua Li[1,2] ✉, Yuanlin Zheng[1,3] ✉ & Xianfeng Chen[1,3,4] ✉

With the advanced development of quantum science, constructing a large-scale quantum network has become a prominent area in the future of quantum information technology. Future quantum networks promise to enable a wide range of groundbreaking applications and to unlock fundamentally new technologies in information security and large-scale computation. The future quantum internet is required to connect quantum information processors to achieve unparalleled capabilities in secret communication and enable quantum communication between any two points on Earth. However, existing quantum networks are primarily designed to facilitate communication between end users within their own networks. Bridging different independent networks to form a fully connected quantum internet has become a pressing challenge for future quantum communication systems. Here we demonstrate the quantum fusion of two independent networks based on multi-user entanglement swapping, to merge two 10-user networks into a larger network with 18 users in a quantum correlation layer. By performing Bell state measurements between two non-neighbouring nodes, users from different networks can establish entanglement, allowing all 18 users to ultimately communicate with each other using the swapped states. Our approach opens up promising opportunities for establishing quantum entanglement between remote nodes across different networks, facilitating versatile quantum information interconnects and enabling the construction of large-scale intercity quantum communication networks.

Driven by the rapid advancement of quantum information technologies[1–6], quantum internet has emerged as a critical objective for quantum information processing[7–11]. The future quantum internet is expected to facilitate a range of innovative quantum technologies and enable secure communication protocols between any two users on a global scale[12–16]. As the paradigmatic quantum mechanical platform, entanglement-based quantum networks enable a wide range of powerful applications such as secure communication[17,18], distributed quantum sensing[19,20] and fundamental tests of quantum mechanics[21–23]. Recently, fully connected quantum communication networks based on quantum entanglement have garnered considerable interest, as this network configuration enables simultaneous communication among multiple users while minimizing infrastructure and hardware requirements[24–27]. It is an important candidate for establishing a fully connected quantum Internet, which may revolutionize the way of information exchange in the future. So far, existing fully connected networks constructed using dense wavelength

[1]State Key Laboratory of Photonics and Communications, School of Physics and Astronomy, Shanghai Jiao Tong University, Shanghai, China. [2]Department of Physics, Shanghai Key Laboratory of Materials Protection and Advanced Materials in Electric Power, Shanghai University of Electric Power, Shanghai, China. [3]Shanghai Research Center for Quantum Sciences, Shanghai, China. [4]Collaborative Innovation Center of Light Manipulation and Applications, Shandong Normal University, Jinan, China. [5]These authors contributed equally: Yiwen Huang, Yilin Yang, Hao Li. ✉e-mail: lyhua1984@shiep.edu.cn; ylzheng@sjtu.edu.cn; xfchen@sjtu.edu.cn

https://doi.org/10.1038/s41566-025-01792-0

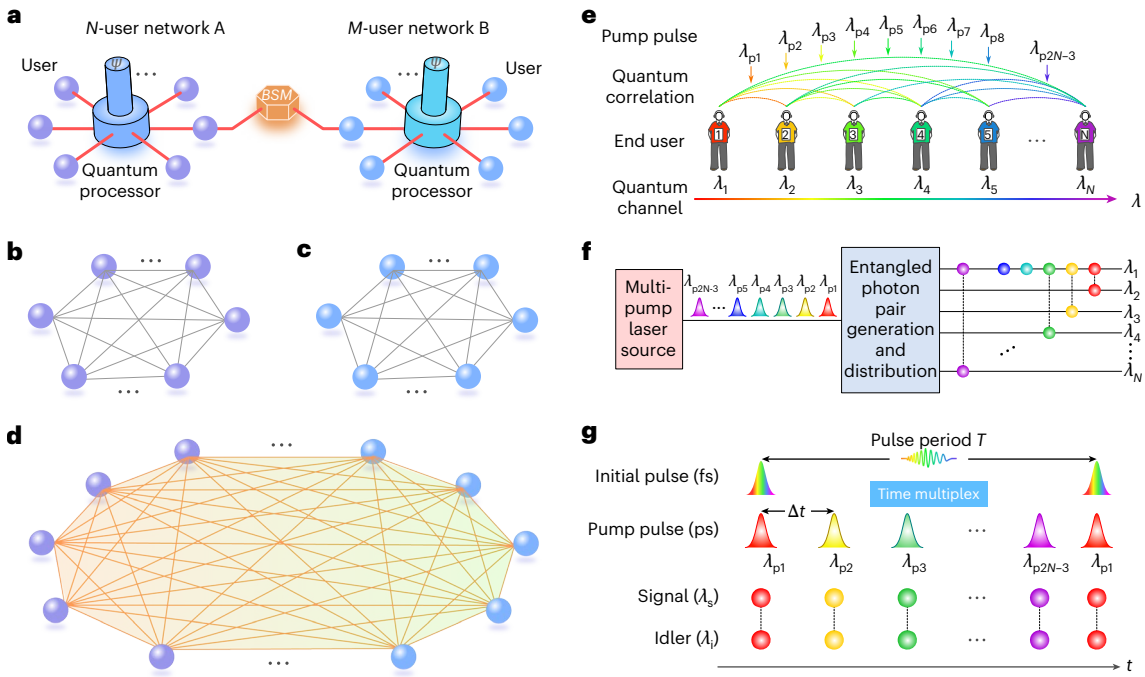

Fig. 1 | Scheme of quantum network fusion, network architecture and operation principle. a, The physical configuration of network fusion based on entanglement swapping. Two fully connected networks send one node to a third party for BSM. **b**,**c**, Topological structures of networks A (**b**) and B (**c**) in the quantum correlation layer. Both the networks have a fully connected logical topology. **d**, The topological structure of the new network after quantum fusion of networks A and B. **e**, The operation principle of the wavelength-multiplexing scheme for the unique design of pump pulses. **f**, Illustration of the entangled photon pair generation and distribution. **g**, The operation principle of the active temporal multiplexing scheme.

division multiplexing (DWDM) have primarily been designed to enable communication between end users within the same network. To enable the communication between the end users in different independent networks in future, an efficient and feasible technique is required for quantum processors to achieve the quantum fusion of two independent networks, which means the two networks are merged into a larger network in the quantum correlation layer.

Entanglement swapping[28–30], which makes two independent quantum entangled states become entangled without direct interaction, provides a promising technology for bridging two independent quantum networks[31–33]. Entanglement swapping between two end nodes in different networks has been developed to connect these networks in a point-to-point topology, enabling communication between the two specific nodes after a Bell state measurement (BSM)[34,35]. However, network fusion based on entanglement swapping of multi-user entangled states, which would enable simultaneous communication among all users in two different networks, has not yet been demonstrated. Implementing the coherent fusion of two independent multi-user networks is extremely important for developing the future quantum internet. Meanwhile, in the existing fully connected networks constructed using the DWDM technique or beam splitters[24–27], the number of quantum correlations and communication links becomes increasingly complex and grows quadratically as the number of users increases, leading to increased system complexity and performance degradation. Implementing Hong–Ou–Mandel (HOM) interference—a prerequisite for entanglement swapping—among multiple users is very challenging in these networks because achieving high-visibility HOM interference requires photons to be indistinguishable in all degrees of freedom, including wavelength[36]. A novel and feasible scheme is needed to overcome this challenge for constructing a large-scale quantum network.

In this work, we present the first experimental demonstration of deterministic network fusion of two independent fully connected networks based on multi-user entanglement swapping. We first develop a scheme—active temporal and wavelength multiplexing (ATWM)—to construct two fully connected 10-user quantum networks, each using a single wavelength channel per end node. By sending one node to a third party for BSM, each pair of users in different networks can generate polarization entanglement after entanglement swapping and the two independent networks are ultimately merged into a larger fully connected quantum network with 18 end nodes. Our approach offers a crucial capability for quantum communication across different networks and is advantageous for building a large-scale quantum internet that enables communication among all users.

Results

Scheme of network fusion and network architecture

Network fusion based on entanglement swapping. Implementing the fusion of two quantum networks involves two main technical challenges. First, two independent networks need to have a fully connected topology so that their users can communicate with each other. Second, high-quality entanglement swapping is required for all the involved entangled states simultaneously. The overall scheme of quantum network fusion based on multi-user entanglement swapping is shown in Fig. 1, which is conceptually illustrated using three layers of abstraction. Figure 1a shows the physical topology of the fused network, which primarily consists of three parts: the physical components of network A, network B and the third-party node Charlie responsible for the BSM. Figure 1b,c illustrates the quantum correlation layers of networks A and B with a fully connected mesh before the network fusion, while Fig. 1d shows the overall quantum correlation layer of the integrated network after the network fusion. The two fully connected networks A and B, consisting of M ($M \geq 2$) and N ($N \geq 2$) end nodes, respectively, are finally merged into a larger fully connected network C with $M+N-2$ end nodes, as shown in Fig. 1d. To establish entanglement between the end nodes of the two quantum networks through entanglement swapping, two end nodes from the two networks respectively are sent to the third-party Charlie to perform a joint measurement, and then the measured results are fed forward to the remaining end nodes of the two

https://doi.org/10.1038/s41566-025-01792-0

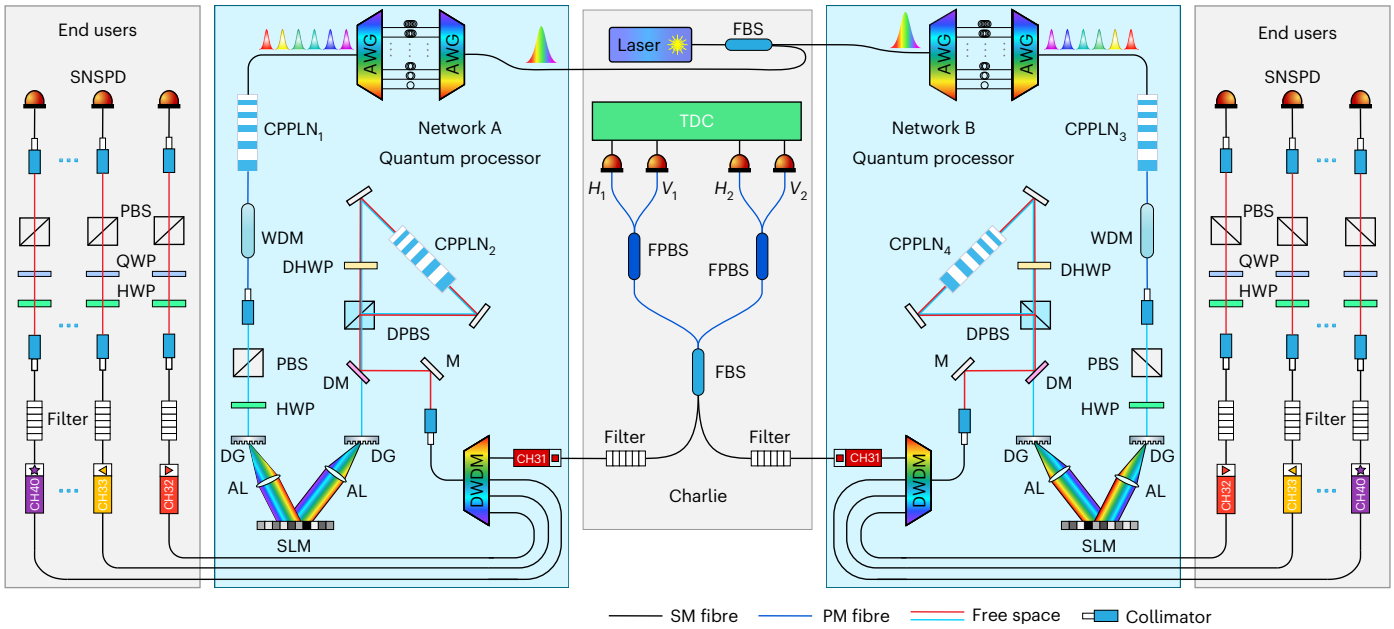

Fig. 2 | Experimental set-up for the network fusion of two fully connected networks. The quantum processors of networks A and B construct the polarization-entangled fully connected networks by using the ATWM scheme. In each network, the femtosecond laser pulses from a mode-locked fibre laser are multiplexed into a series of pump pulses and are frequency-doubled in a CPPLN waveguide. After passing through a phase compensator, the produced second harmonics create entangled photon pairs in the second CPPLN waveguide in a Sagnac loop. The quantum processor allocates the entangled photons to the end nodes using an ITU DWDM filter and sends one link to Charlie, which performs the BSM using a combination of a 50/50 FBS, fibre polarization beam splitters (FPBS) and SNSPDs. TDC, time-to-digital converter; AWG, arrayed waveguide grating; WDM, wavelength division multiplexing filter; HWP, half-wavelength plate; QWP, quarter-wave plate; DG, diffraction grating; AL, achromatic lens; DM, dichroic mirror; DPBS, dual-wavelength PBS; PM, polarization-maintaining; SM, single-mode; DHWP, dual-wavelength half-wave plate.

networks. By quantum entanglement swapping, two multi-user entangled networks consisting of M and N quantum nodes, respectively, can be merged into a new larger multi-user entangled network consisting of $M+N-2$ quantum nodes.

ATWM scheme. To construct an N-user network with a fully connected graph in the quantum correlation, the quantum processor needs to prepare a minimum of $N(N-1)/2$ links to allocate them to the end users. Different from pre-existing networks, which allocate the entangled photon pairs to different users by using dense wavelength division multiplexers or beam splitters, we achieve the fully connected topology of the network by directly pumping a nonlinear waveguide based on the ATWM scheme. The principle of our demonstration is illustrated in Fig. 1e–g. In our network, each user receives only one wavelength channel which consists of $N-1$ temporally separate photons entangled with other $N-1$ users, respectively. The central wavelength of the quantum channel for the user N is defined as λ_N. As shown in Fig. 1e, the quantum processor designs $2N-3$ pump pulses with the central wavelengths of λ_{p1} to λ_{p2N-3}, respectively, where $\lambda_{p2N-3}=1/(\frac{1}{\lambda_{N-1}}+\frac{1}{\lambda_N})$. Due to energy conservation during the spontaneous parametric down-conversion (SPDC) process, the downconverted photon pairs are naturally frequency–time entangled and their spectra are symmetric with respect to the central wavelength of their pump wavelength. Due to the unique design of the pump wavelengths, all the symmetric wavelength channels for the end users can share a different entangled state with each other, creating the fully connected graph of the network. Figure 1f conceptually illustrates the generation and distribution of quantum entanglement in the network. A train of tailored pump pulses, specifically designed in both wavelength and time domains, is used to generate quantum entangled photon pairs through SPDC processes. The entangled photon pairs are then distributed to the end users via the quantum channels, and each user receives one wavelength channel consisting of $N-1$ temporally separate photons entangled with other $N-1$ users, respectively. To effectively distinguish different photon pairs, we use the temporal multiplexing scheme to separate different pump pulses with a time interval of Δt, as shown in Fig. 1g. As a result, the downconverted photon pairs are also separated in the time domain by the same time interval.[37]. Then, one can distinguish different entangled states according to the photon arrival time, which improves the signal-to-noise ratio of the quantum system. A key technique in the ATWM scheme is ensuring that all involved pump lasers can generate entangled photon pairs through the SPDC process. We take advantage of the type-zero chirped quasi-phase-matching configuration and the high-efficiency property of the lithium niobate-on-insulator ridge waveguides to achieve this scheme.

Experimental set-up and network performance

To demonstrate the versatility and flexibility of our approach, we perform network fusion on two independent polarization-entangled networks, each with ten users. The experimental set-up is depicted in Fig. 2. A femtosecond laser with a repetition frequency of 60 MHz is first divided into two parts by a 50:50 fibre beam splitter (FBS) and then sent to the quantum processors A and B to construct the fully connected networks using the ATWM scheme. The second harmonics of pump lasers with specific design in wavelengths and time domain are injected into a chirped periodically poled lithium niobate (CPPLN) waveguide (Supplementary Section I) to generate polarization Einstein–Podolsky–Rosen (EPR) pairs in the Bell state $|\phi^+\rangle_n=1/\sqrt{2}(|H\rangle_s|H\rangle_i+|V\rangle_s|V\rangle_i)$, via SPDC processes in a Sagnac loop, where n is the wavelength number of the pump pulses, and s and i denote signal and idler photons, respectively. Finally, a thin-film DWDM filter is utilized to divide the entangled photons and allocate the unique International Telecommunication Union (ITU) channels to the end users. The details of the experimental set-up are provided in the Methods. Due to the unique design of the pump lasers and high efficiency of the CPPLN waveguides, each pair of quantum channels shares one pair of entangled photons with each other, forming a fully connected mesh in the quantum correlation layer of the network.

https://doi.org/10.1038/s41566-025-01792-0

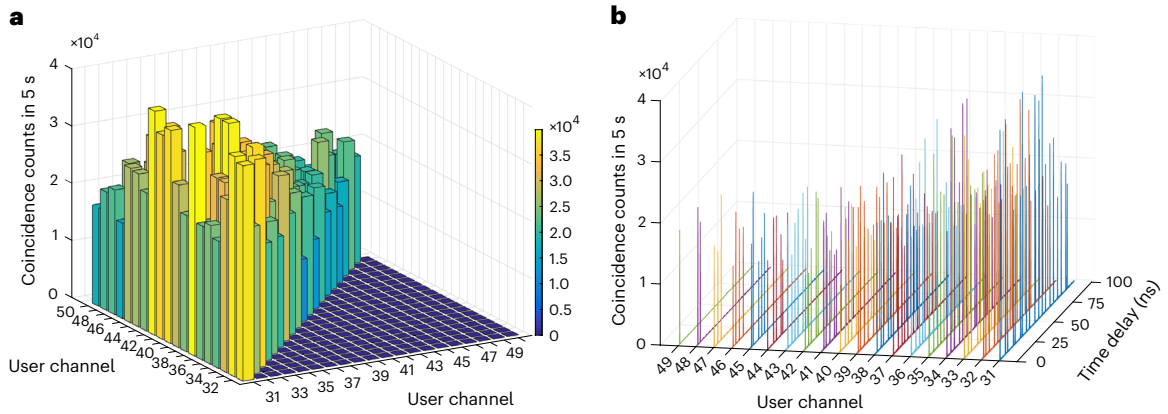

Fig. 3 | Experimental results of the fully connected network constructed using the ATWM scheme. a, Measured two-photon coincidence counts between each pair of end users. **b**, Temporal cross-correlations between the time traces of all the 20 users. Each cross-correlation peak represents a pair of entangled photons shared by each pair of end users in the network.

Before demonstrating the network fusion based on multi-user entanglement swapping, we first investigate the performance of the fully connected network constructed using the proposed ATWM scheme. To show the advancement of our scheme, we construct a 20-user network as a demonstration. During this experiment, a total of 37 pump pulses with central wavelengths varying from 1,552.12 nm to 1,537.79 nm are used to generate the correlative photon pairs via the SPDC process in the $CPPLN_2$ waveguide. A DWDM filter with ITU channels of CH31 to CH50 are leveraged to allocate the downconverted photons to the end users, respectively. To characterize the performance of the constructed network, we measure the coincidence counts between the 20 users after the entanglement distribution. The measurements are performed simultaneously for every ten users owing to the limited detection equipment, and the downconverted mean photon number for each photon pair is controlled to be $\mu \approx 0.01$ per pulse. The experimental results are shown in Fig. 3a, in which any two users have coincidence events with a count rate over 10^4 in 5 s. This means that any two users share one pair of entangled photons with each other, indicating a fully connected topological graph has been established. Due to the ATWM scheme, the end users can easily identify the entangled photons generated during each SPDC process and are able to calculate the coincidence count according to the photon arrival time. Figure 3b shows all the temporal cross-correlation functions among the 20 end users. The cross-correlation peaks in the column of CH31 (N) are the coincidence counts with CH32 ($N+1$) to 50 under different delay times calculated by taking detection results of CH31 (N) as the reference signal. These results confirm our proposed scheme can be used to construct a large-scale quantum network with a fully connected topology structure. Our proposed fully connected network can be encoded using time-bin (Supplementary Section II) and polarization degrees of freedom.

To guarantee the high quality of the entanglement swapping, it is crucial for each network to ensure the end users share high-quality polarization-entangled states with other users. The quantum processors first construct their ten-user polarization-entangled networks using the ATWM scheme as mentioned above. At this time, only 17 pump pulses with the central wavelength varying from 1,552.12 nm to 1,545.7 nm are used to pump the CPPLN waveguides and the end users' channels turn into CH31 to CH40 for each network. To characterize the received polarization-entangled states, each user in two networks is equipped with a superconducting nanowire single-photon detector (SNSPD) and a polarization state analyser consisting of a half-wavelength plate, a quarter-wave plate and a PBS. We investigate the polarization entanglement of the networks by measuring the two-photon interference fringes in two mutually unbiased bases $|H\rangle$ / $|V\rangle$ and $|D\rangle$ / $|A\rangle$ using the standard two-photon interference technique[38]. Figure 4a,b shows the typical interference fringes between CH31 and other users in networks A and B, respectively. The visibility of the interference fringes for each state was measured to be above 95%, exceeding the 70.7% local bound of Bell's inequality[39], and reveals the existence of polarization entanglement in all available channel pairs. We calculate the fidelities of all the involved states in two networks as compared with the ideal Bell state $|\phi^+\rangle = 1/\sqrt{2}(|H\rangle_s|H\rangle_i + |V\rangle_s|V\rangle_i)$ and find that the fidelities exceed 96% for all measured channel pairs, laying a solid foundation for high-quality network fusion based on entanglement swapping.

Realization of multi-user entanglement swapping

Next, we demonstrate the quantum fusion of the two polarization-entangled fully connected networks by performing multi-user entanglement swapping. To merge the two 10-user networks into an 18-user network in quantum correlation layer, both the quantum processors send the channel CH31 to the third-party Charlie to perform the BSM by interfering them on an FBS, as shown in Fig. 2. To enable the communication between each pair of the users in two independent networks, one needs to establish entanglement between all the end nodes that never interacted by entanglement swapping. This requires a high-visibility HOM interference between all the involved photons corresponding to each quantum state in CH31 from the two networks. Due to the ATWM scheme, each end node uses only a single wavelength channel, and every quantum state can be distinguished based on photon arrival time, providing the necessary condition for high-visibility HOM interference among multiple users simultaneously. The two network providers can achieve the entanglement swapping between any two users from different networks by carefully adjusting the delay of pump pulses to overlap the corresponding CH31 signals on the FBS.

As a reliability check before performing the experimental test of bilocal hidden variable models for the swapped entangled pairs, we first measure the HOM interference for the two networks. To achieve a high-visibility interference between two networks, we exploit two kinds of narrow-band grating filter with a bandwidth of 0.1 nm and 0.2 nm for CH31 photons and other channels, respectively, to suppress the spectral distinguishability. See Supplementary Section III for further details about the experimental settings. The measured HOM interferences are shown in Fig. 5, in which Fig. 5c–k and Fig. 5l–t are the HOM interferences for the time settings in Fig. 5a and Fig. 5b, respectively. The visibilities defined as $V_{\mathrm{dip}} = 1 - R_0/R_t$, where R_0 and R_t are fitted counts at zero and infinite delays, respectively, are found to be over 75% for all the entangled state, with the highest and average

https://doi.org/10.1038/s41566-025-01792-0

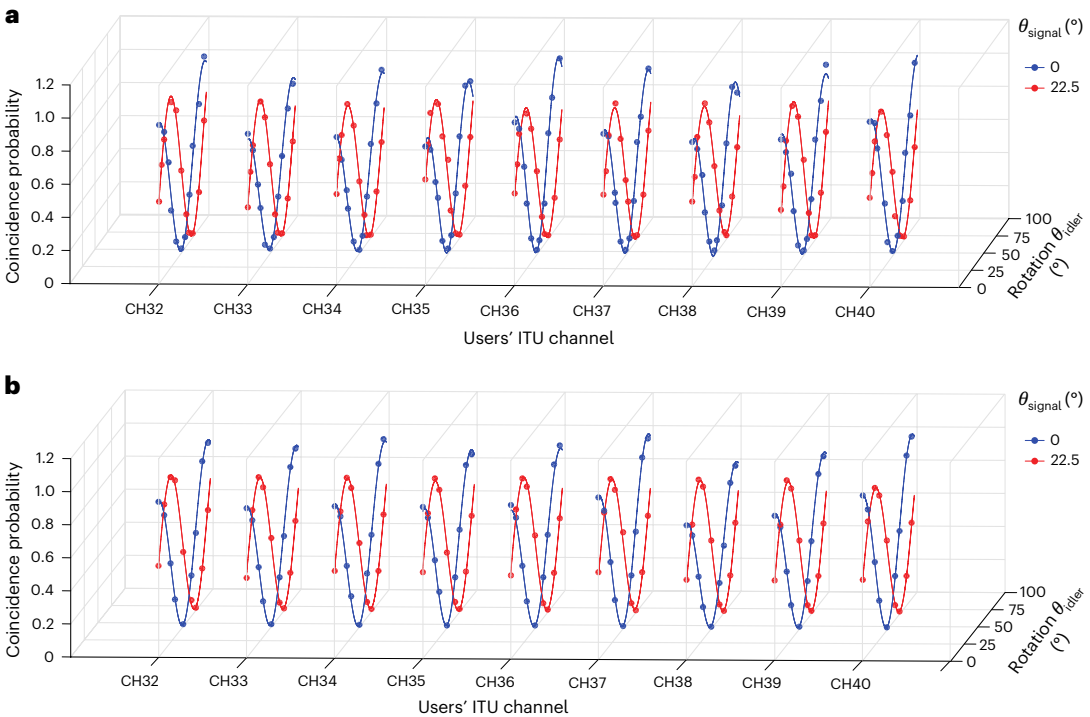

Fig. 4 | Experimental two-photon interference for polarization entanglement between CH31 and other users in the two networks. **a**, Two-photon coincidence count as a function of signal polarization under two non-orthogonal projection bases for network A. **b**, Two-photon coincidence count as a function of signal polarization under two non-orthogonal projection bases for network B.

visibilities of 90.7% and (83.5 ± 3.4)%, respectively, which break the classical boundary of 50%.

Characterization of the entangled states

We confirm successful entanglement swapping of two networks by testing the entanglement of the previously uncorrelated photons for all the involved photon pairs. The specific states of the swapped entangled pairs depend on the result of the BSM. Consider the successful generation of both initial entangled states $|\phi^+\rangle_n = 1/\sqrt{2}(|H\rangle_{\mathrm{CH31_A}}|H\rangle_{\lambda_n} + |V\rangle_{\mathrm{CH31_A}}|V\rangle_{\lambda_n})$ and $|\phi^+\rangle_m = 1/\sqrt{2}(|H\rangle_{\mathrm{CH31_B}}|H\rangle_{\lambda_m} + |V\rangle_{\mathrm{CH31_B}}|V\rangle_{\lambda_m})$, where $\mathrm{CH31_A}$ and $\mathrm{CH31_B}$ represent the CH31 photons from networks A and B, respectively, and λ_n and λ_m represent the correlated idler photons in CH32 to CH40 of networks A and B. When overlapping the photons $\mathrm{CH31_A}$ and $\mathrm{CH31_B}$ on the FBS, the overall states of the entangled photon pairs would be cast into

$$\begin{aligned}|\psi\rangle = |\phi^+\rangle_n \otimes |\phi^+\rangle_m = \frac{1}{2}\left(|H\rangle_{\mathrm{CH31_A}}|H\rangle_{\lambda_n} + |V\rangle_{\mathrm{CH31_A}}|V\rangle_{\lambda_n}\right)\\ \otimes\left(|H\rangle_{\mathrm{CH31_B}}|H\rangle_{\lambda_m} + |V\rangle_{\mathrm{CH31_B}}|V\rangle_{\lambda_m}\right) = \frac{1}{2}\left(|\phi^+\rangle_{\mathrm{CH31_A CH31_B}}|\phi^+\rangle_{\lambda_n\lambda_m}\right.\\ +|\phi^-\rangle_{\mathrm{CH31_A CH31_B}}|\phi^-\rangle_{\lambda_n\lambda_m} + |\psi^+\rangle_{\mathrm{CH31_A CH31_B}}|\psi^+\rangle_{\lambda_n\lambda_m}\\ \left.+|\psi^-\rangle_{\mathrm{CH31_A CH31_B}}|\psi^-\rangle_{\lambda_n\lambda_m}\right).\end{aligned} \quad (1)$$

Charlie implements the BSM by HOM interference at a 50/50 FBS and subsequent two fibre polarization beam splitters, as shown in Fig. 2. With these experimental configurations, one can discriminate two of the four Bell states $|\psi^+\rangle_{\mathrm{CH31_A CH31_B}} = 1/\sqrt{2}(|H\rangle_{\mathrm{CH31_A}}|V\rangle_{\mathrm{CH31_B}} + |V\rangle_{\mathrm{CH31_A}}|H\rangle_{\mathrm{CH31_B}})$ and $|\psi^-\rangle_{\mathrm{CH31_A CH31_B}} = 1/\sqrt{2}(|H\rangle_{\mathrm{CH31_A}}|V\rangle_{\mathrm{CH31_B}} - |V\rangle_{\mathrm{CH31_A}}|H\rangle_{\mathrm{CH31_B}})$, which is the optimum efficiency possible with linear optics. A twofold coincidence detection event between either D_{H_1} and D_{V_2} or D_{V_1} and D_{H_2} indicates a projection on $|\psi^-\rangle_{\mathrm{CH31_A CH31_B}}$, while a coincidence detection event between either D_{H_1} and D_{V_1} or D_{H_2} and D_{V_2} indicates a projection on $|\psi^+\rangle_{\mathrm{CH31_A CH31_B}}$. It is worth noting that the BSM results for different photon pairs can be easily identified according to the photon arrival time owing to the ATWM scheme. We select the Bell state $|\psi^-\rangle_{\mathrm{CH31_A CH31_B}}$ as an example to demonstrate the multi-user entanglement swapping between two networks. Measuring two-photon interference under two mutually unbiased bases can detect whether the quantum state has breaking inequalities. We control the projection basis of idle photons in network A as $|H\rangle$ / $|V\rangle$ and $|D\rangle$ / $|A\rangle$, respectively, and measure the statistical quadruple coincidence counts by scanning the half-wave plate angle of idle photons in network B. The typical experimental results are shown in the Fig. 6. We obtain the average visibilities of the interference fringes to be $V_{\mathrm{swapped}} = (R_{\max} - R_{\min})/(R_{\max} + R_{\min}) = (81.2 \pm 2.0)\%$ and $(79.8 \pm 5.5)\%$ for the swapped entangled pairs $\mathrm{CH32_A}$ and $\mathrm{CH32_B}$ and $\mathrm{CH32_A}$ and $\mathrm{CH33_B}$, respectively, for the temporal settings in Fig. 5a and Fig. 5b. The visibility achieved in our experiment clearly exceeds the classical bound of the CHSH inequality, revealing polarization entanglement between the swapped entangled pairs. Moreover, we calculate the fidelities of the entangled states after the entanglement swapping using $F = (3V_{\mathrm{swapped}} + 1)/4$. The typical results are shown in Fig. 6c, in which one can obtain an average fidelity of $(84.5 \pm 2)\%$. These results prove that polarization entanglement can be generated between the previously uncorrelated users in two networks by controlling the delay of pump pulses to overlap the signal photons of different photon pairs on the FBS. Ultimately, the two 10-user fully connected networks are merged into an 18-user network in the quantum correlation layer after the multi-user entanglement swapping. All the end users can communicate with each other using the entanglement-based quantum key distribution protocol. See Supplementary Section IV for the analysis of quantum key distribution between each pair of users in the fused 18-user network.

Discussion

Here, we highlight the substantial advantages of our approach. First, our proposed fully connected quantum networks based on ATWM scheme have a distinct advantage in scalability and signal-to-noise ratio over the existing networks constructed using DWDM technique or beam

https://doi.org/10.1038/s41566-025-01792-0

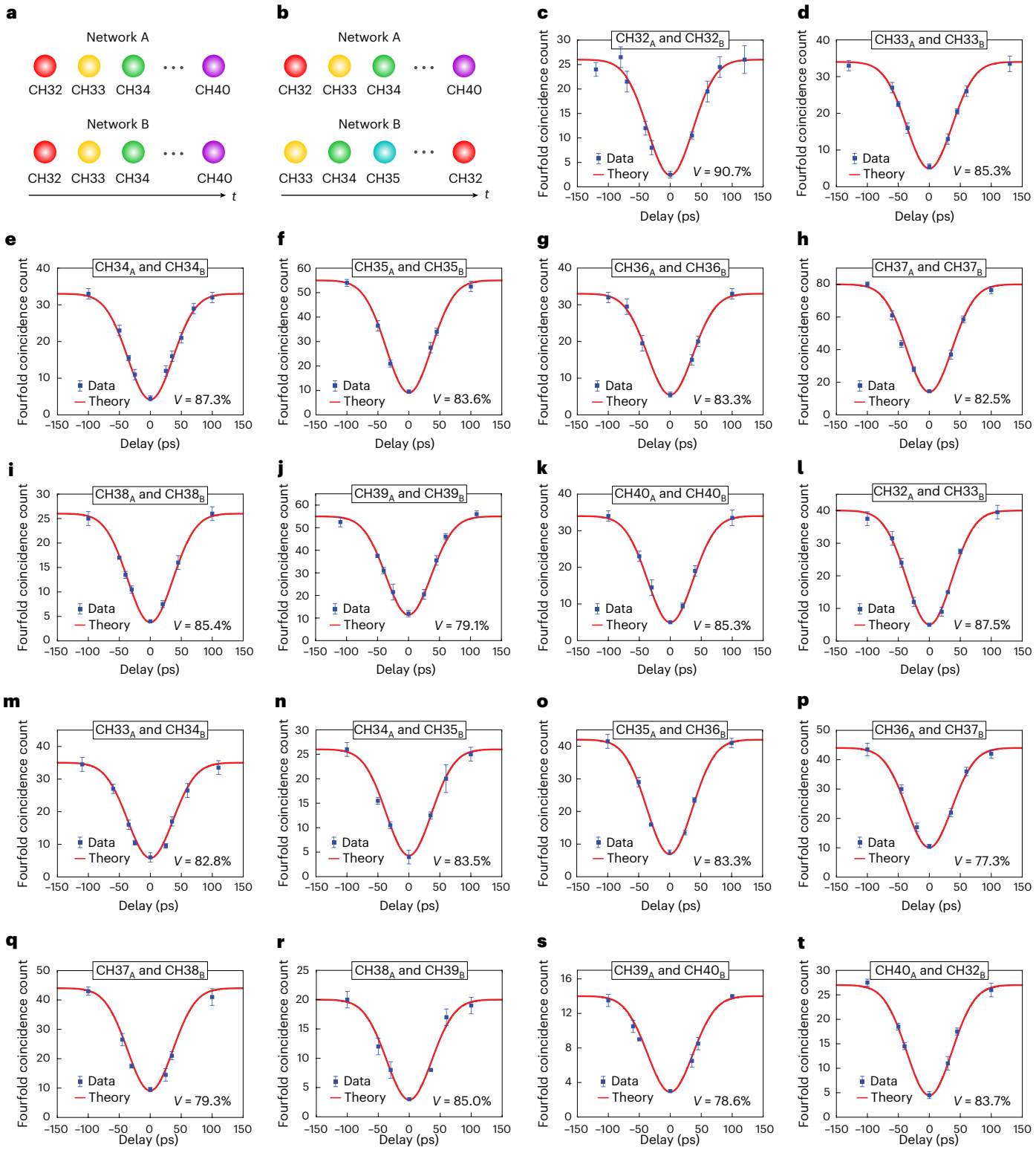

Fig. 5 | Experimental HOM interference under two different delays. a, Temporal distribution of the CH31 photons correlated with different channels from the two networks. The CH31 photons of the photon pairs $\{CH31_A, CH32_A\}$ and $\{CH31_B, CH32_B\}$, $\{CH31_A, CH33_A\}$ and $\{CH31_B, CH33_B\}$, …, and $\{CH31_A, CH40_A\}$ and $\{CH31_B, CH40_B\}$ are temporally overlapping at the FBS, respectively. **b**, Temporal distribution of the CH31 photons correlated with different channels from the two networks. The CH31 photons of the photon pairs $\{CH31_A, CH32_A\}$ and $\{CH31_B, CH33_B\}$, $\{CH31_A, CH33_A\}$ and $\{CH31_B, CH34_B\}$, …, and $\{CH31_A, CH40_A\}$ and $\{CH31_B, CH32_B\}$ have the same temporal distribution, respectively. Channels in the same vertical column indicate that the CH31 photons correlated with these channels overlap at the FBS, achieved by controlling the temporal distribution of pump pulses in the quantum processors. **c**–**k**, HOM interference for different photon pairs under the temporal distribution of the CH31 photons shown in **a**. The heading $CH32_A$ and $CH32_B$ at the top of **c** corresponds to the photon pairs $\{CH31_A, CH32_A\}$ and $\{CH31_B, CH32_B\}$ and so on. **l**–**t**, HOM interference for different photon pairs under the temporal distribution of the CH31 photons shown in **b**. The heading $CH32_A$ and $CH33_B$ at the top of **l** corresponds to the photon pairs $\{CH31_A, CH32_A\}$ and $\{CH31_B, CH33_B\}$ and so on. Each fourfold coincidence count is measured for 400 s, and the error bars indicate one standard deviation.

https://doi.org/10.1038/s41566-025-01792-0

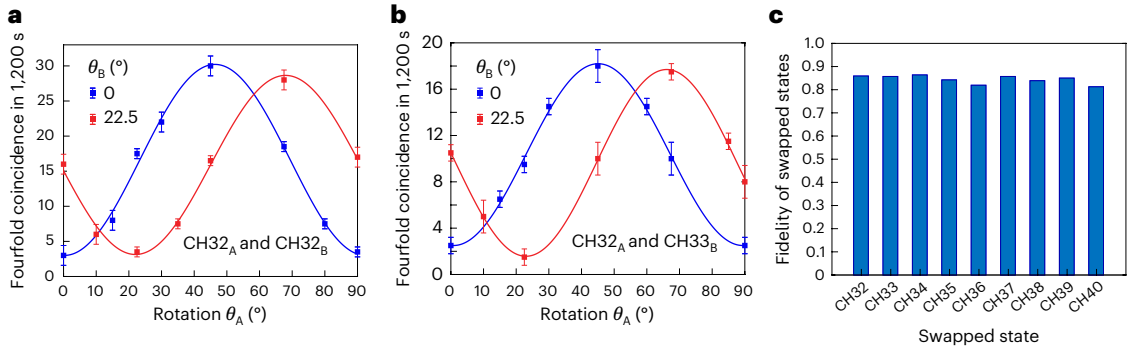

Fig. 6 | Experimental two-photon interference for polarization entanglement after multi-user entanglement swapping. a, Fourfold coincidence counts as a function of signal polarization for the swapped photon pair CH32$_A$ and CH32$_B$. **b**, Fourfold coincidence counts as a function of signal polarization for the swapped photon pair CH32$_A$ and CH33$_B$. **c**, Measured fidelities of the swapped states. CH32 to CH40 on the *x* axis represent the swapped states of CH32$_A$ and CH32$_B$ to CH40$_A$ and CH40$_B$, respectively. The error bars indicate one standard deviation.

splitters. To add a new user into the latter, the quantum processor needs to multiplex a large number of quantum channels into each user's fibre, requiring considerable modifications to the quantum system. In our scheme, only two more wavelength lasers are required to multiplex into the pump pulses for the SPDC processes, thanks to photon energy conservation. Besides, owing to the ingenious design of the pump pulses in temporal domain, the SPDC photons generated by different pump pulses can be detected in different photon time slots and the end users can clearly distinguish the photon detection results of each entangled state according to the photon arrival time. This characteristic would improve the signal-to-noise ratio and enable the end users' two-party communication. Moreover, our proposed network has the nearly lowest system loss and most compact system architecture because only one DWDM filter is need to allocate the entangled photons to the end users. These salient characteristics make the ATWM scheme more suitable to construct a large-scale fully connected network. Second, each user contains only one wavelength channel, which is conducive to subsequent quantum operations, such as quantum interference and frequency upconversion for quantum storage. Last, but most importantly, our proposed network fusion scheme based on multi-user entanglement swapping enables the connection of the remote users in different networks, merging two independent networks into a larger network. This approach can realize mutual communication between all users in different networks, which has important application prospects in constructing large-scale quantum networks in the future.

However, it cannot be denied that the ATWM scheme is not optimal in terms of resource requirements. For an *N*-user network with a fully connected graph in the quantum correlation, the quantum processor designs $2N-3$ pump pulses to pump the nonlinear waveguides, and only the entangled photon pairs shared among the *N* users are utilized to construct the fully connected network structure. The quantum resources whose wavelengths are not the specific wavelength channels of the *N* users are underused. To make better use of quantum resources, we design an optimal scheme to construct a fully connected network with more end users by combining the ATWM scheme and DWDM technology. In this scheme, by taking advantage of the DWDM technology, the *N*-user fully connected network is capable of expanding to a larger one with $2N-3$ end users while keeping the pump pulses unchanged; see also Supplementary Section V for more details about the optimized scheme.

Another prospective improvement of the networks can be realized by utilizing more narrow-band photons to constructed the fully connected network architecture, which can potentially increase the efficiency of quantum storage and improve the interference visibility of entanglement swapping. An alternative method is exploiting narrow-band filters with a narrower bandwidth to deal with the pump lasers and the entangled photons[23]. In this case, to achieve the best system signal-to-noise ratio and secure key generation rate, a trade-off optimization of the pump power is required to balance the brightness of entangled photon pairs and multiphoton effects. Another feasible approach is to directly generate narrow-band photon pairs with central wavelengths and free spectral ranges matching ITU channels, using cavity-enhanced SPDC or spontaneous four-wave mixing processes in integrated quantum photonic devices, such as high-quality periodically poled thin-film lithium niobate microring[40] and silicon nitride microring chips[29,41].

An interesting question is how to extend the proposed network fusion scheme to longer distances while maintaining the networks' performance. To overcome the distance limit of quantum communication owing to the fibre loss, quantum repeaters[42] mainly including components of quantum memory, entanglement swapping and distillation, enable the entangled states to be distributed with a polynomial scaling in the distance, which facilitates the implementation of extending our network scheme to larger distances in the future. The most critical challenge in realizing practical long-distance quantum repeater networks is the establishment of robust entanglement between remote quantum memory nodes. Although great progress has been made in quantum memory in recent years[43,44], it is still challenging to realize large-scale and long-distance practical quantum communication networks using quantum repeaters with the capabilities of current technology. Another promising approach to extend the fully connected networks constructed by the ATWM scheme to long distances is using the all-photonic quantum repeaters[45]. By harnessing repeater graph states in different repeater nodes processed by linear optical elements, all-photonic quantum repeaters are expected to enable the implementation of long-distance quantum networks while substantially reducing the reliance on quantum memory[46–48]. The combination of all-photonic quantum repeaters and the ATWM scheme would provide a potential solution implementing long-distance multi-user fully connected networks and quantum fusion of remote networks towards scalable quantum internet.

Conclusion

In summary, we have successfully realized the quantum fusion of two independent 10-user networks based on multi-user entanglement swapping, merging them into a larger network with 18 users in the quantum correlation layer. The results show that the proposed ATWM scheme can be used to construct high-performance larger-scale networks with a fully connected topological structure. By performing the BSM between two end nodes, the users from different networks can establish entanglement after entanglement swapping, ultimately enabling every pair among the 18 users to communicate with each other. Our approach opens attractive opportunities for the establishment of quantum entanglement between remote nodes in different networks, which facilitates versatile quantum information interconnects and

has great application in constructing large-scale intercity quantum communication networks.

Online content

Any methods, additional references, Nature Portfolio reporting summaries, source data, extended data, supplementary information, acknowledgements, peer review information; details of author contributions and competing interests; and statements of data and code availability are available at https://doi.org/10.1038/s41566-025-01792-0.

References

1. Xu, F., Ma, X., Zhang, Q., Lo, H. K. & Pan, J. W. Secure quantum key distribution with realistic devices. *Rev. Mod. Phys.* **92**, 025002 (2020).
2. Li, W. et al. High-rate quantum key distribution exceeding 110 Mb s^{-1}. *Nat. Photonics* **17**, 416–421 (2023).
3. Grünenfelder, F. et al. Fast single-photon detectors and real-time key distillation enable high secret-key-rate quantum key distribution systems. *Nat. Photonics* **17**, 422–426 (2023).
4. Humphreys, P. C. et al. Deterministic delivery of remote entanglement on a quantum network. *Nature* **558**, 268–273 (2018).
5. Wang, S. et al. Twin-field quantum key distribution over 830-km fibre. *Nat. Photonics* **16**, 154–161 (2022).
6. Zhong, Y. et al. Deterministic multi-qubit entanglement in a quantum network. *Nature* **590**, 571–575 (2021).
7. Kržič, A. et al. Towards metropolitan free-space quantum networks. *NPJ Quantum Inf.* **9**, 95 (2023).
8. Ribezzo, D. et al. Deploying an inter-European quantum network. *Adv. Quantum Technol.* **6**, 2200061 (2023).
9. Chen, Y. A. et al. An integrated space-to-ground quantum communication network over 4,600 kilometres. *Nature* **589**, 214–219 (2021).
10. Li, Y. et al. Multiuser time-energy entanglement swapping based on dense wavelength division multiplexed and sum-frequency generation. *Phys. Rev. Lett.* **123**, 250505 (2019).
11. Pompili, M. et al. Realization of a multinode quantum network of remote solid-state qubits. *Science* **372**, 259–264 (2021).
12. Wehner, S., Elkouss, D. & Hanson, R. Quantum internet: a vision for the road ahead. *Science* **362**, eaam9288 (2018).
13. Wei, S.-H. et al. Towards real-world quantum networks: a review. *Laser Photonics Rev.* **16**, 2100219 (2022).
14. Simon, C. Towards a global quantum network. *Nat. Photonics* **11**, 678–680 (2017).
15. Pittaluga, M. et al. Long-distance coherent quantum communications in deployed telecom networks. *Nature* **640**, 911–917 (2025).
16. Chang, X. Y. et al. Hybrid entanglement and bit-flip error correction in a scalable quantum network node. *Nat. Phys.* **21**, 583–589 (2025).
17. Hermans, S. L. N. et al. Qubit teleportation between non-neighbouring nodes in a quantum network. *Nature* **605**, 663–668 (2022).
18. Cacciapuoti, A. S. et al. Quantum internet: networking challenges in distributed quantum computing. *IEEE Network* **34**, 137–143 (2019).
19. Degen, C. L., Reinhard, F. & Cappellaro, P. Quantum sensing. *Rev. Mod. Phys.* **89**, 035002 (2017).
20. Guo, X. et al. Distributed quantum sensing in a continuous-variable entangled network. *Nat. Phys.* **16**, 281–284 (2020).
21. Polino, E. et al. Experimental nonclassicality in a causal network without assuming freedom of choice. *Nat. Commun.* **14**, 909 (2023).
22. Wang, N. N. et al. Certification of non-classicality in all links of a photonic star network without assuming quantum mechanics. *Nat. Commun.* **14**, 2153 (2023).
23. Sun, Q. C. et al. Experimental demonstration of non-bilocality with truly independent sources and strict locality constraints. *Nat. Photonics* **13**, 687–691 (2019).
24. Wengerowsky, S., Joshi, S. K., Steinlechner, F., Hübel, H. & Ursin, R. An entanglement-based wavelength multiplexed quantum communication network. *Nature* **564**, 225–228 (2018).
25. Joshi, S. K. et al. A trusted node-free eight-user metropolitan quantum communication network. *Sci. Adv.* **6**, eaba0959 (2020).
26. Liu, X. et al. An entanglement-based quantum network based on symmetric dispersive optics quantum key distribution. *APL Photonics* **5**, 076104 (2020).
27. Kim, J. H., Chae, J. W., Jeong, Y. C. & Kim, Y. H. Quantum communication with time-bin entanglement over a wavelength-multiplexed fiber network. *APL Photonics* **7**, 016106 (2022).
28. Pan, J. W., Bouwmeester, D., Weinfurter, H. & Zeilinger, A. Experimental entanglement swapping: entangling photons that never interacted. *Phys. Rev. Lett.* **80**, 3891 (1998).
29. Samara, F. et al. Entanglement swapping between independent and asynchronous integrated photon-pair sources. *Quantum Sci. Technol.* **6**, 045024 (2021).
30. Liu, S., Lou, Y., Chen, Y. & Jing, J. All-optical entanglement swapping. *Phys. Rev. Lett.* **128**, 060503 (2022).
31. Kaltenbaek, R., Prevedel, R., Aspelmeyer, M. & Zeilinger, A. High-fidelity entanglement swapping with fully independent sources. *Phys. Rev. A* **79**, 040302 (2009).
32. Lu, C. Y., Yang, T. & Pan, J. W. Experimental multiparticle entanglement swapping for quantum networking. *Phys. Rev. Lett.* **103**, 020501 (2009).
33. Shchukin, E. & van Loock, P. Optimal entanglement swapping in quantum repeaters. *Phys. Rev. Lett.* **128**, 150502 (2022).
34. Guccione, G. et al. Connecting heterogeneous quantum networks by hybrid entanglement swapping. *Sci. Adv.* **6**, eaba4508 (2020).
35. Sun, Q. C. et al. Entanglement swapping over 100 km optical fiber with independent entangled photon-pair sources. *Optica* **4**, 1214–1218 (2017).
36. Hong, C. K., Ou, Z. Y. & Mandel, L. Measurement of subpicosecond time intervals between two photons by interference. *Phys. Rev. Lett.* **59**, 2044 (1987).
37. Xiong, C. et al. Active temporal multiplexing of indistinguishable heralded single photons. *Nat. Commun.* **7**, 10853 (2016).
38. Kwiat, P. G. et al. New high-intensity source of polarization-entangled photon pairs. *Phys. Rev. Lett.* **75**, 4337 (1995).
39. Clauser, J. F., Horne, M. A., Shimony, A. & Holt, R. A. Proposed experiment to test local hidden-variable theories. *Phys. Rev. Lett.* **23**, 880 (1969).
40. Ma, Z. et al. Ultrabright quantum photon sources on chip. *Phys. Rev. Lett.* **125**, 263602 (2020).
41. Fan, Y. et al. Multi-wavelength quantum light sources on silicon nitride micro-ring chip. *Laser Photonics Rev.* **17**, 2300172 (2023).
42. Azuma, K. et al. Quantum repeaters: from quantum networks to the quantum internet. *Rev. Mod. Phys.* **95**, 045006 (2023).
43. Liu, J. et al. Creation of memory–memory entanglement in a metropolitan quantum network. *Nature* **629**, 579–585 (2024).
44. Knaut, C. M. et al. Entanglement of nanophotonic quantum memory nodes in a telecom network. *Nature* **629**, 573–578 (2024).
45. Azuma, K., Tamaki, K. & Lo, H. K. All-photonic quantum repeaters. *Nat. Commun.* **6**, 1–7 (2015).
46. Hasegawa, Y. et al. Experimental time-reversed adaptive Bell measurement towards all-photonic quantum repeaters. *Nat. Commun.* **10**, 378 (2019).
47. Li, Z. D. et al. Experimental quantum repeater without quantum memory. *Nat. Photonics* **13**, 644–648 (2019).
48. Li, B., Goodenough, K., Rozpędek, F. & Jiang, L. Generalized quantum repeater graph states. *Phys. Rev. Lett.* **134**, 190801 (2025).

Methods

Multi-wavelength polarization-entangled photon-pair source

To construct polarization-entangled fully connected networks using the ATWM scheme, we develop a special polarization-entangled source based on a polarization compensator and a Sagnac loop, as shown in Fig. 2, to generate the EPR Bell states $|\phi^+\rangle = 1/\sqrt{2}(|H\rangle_s|H\rangle_i + |V\rangle_s|V\rangle_i)$ for all the pump pulses. In the physical topology layer of each quantum processor, the femtosecond laser pulses are multiplexed into a series of pump pulses with the wavelength and time intervals of $\Delta\lambda_p = 0.4$ nm and $\Delta t \approx 300$ ps, respectively, using arrayed waveguide gratings whose central wavelengths are identified by the ITU. Then, the pump pulses are frequency doubled in a CPPLN waveguide by second-harmonic generation (SHG). The CPPLN waveguides are fabricated by using the method of ultraviolet lithography and deep dry etching[49] and enable effective SHG with over 15-nm pump wavelength range (Supplementary Section I). The residual pump pulses are suppressed by a wavelength division multiplexing filter with an extinction ratio of 180 dB. The multi-wavelength second-harmonic lasers first go through a Fourier-transform set-up that consists of two diffraction gratings, two achromatic lens and a spatial light modulator (SLM) to compensate the polarization and phase of different wavelength pulses. The photons with diagonal polarization are first spectrally dispersed by a grating and then focused to an elongated spot with the wavelength varying from λ_{min} to λ_{max} by an achromatic lens. A horizontal SLM with a resolution of 1,920 × 1,200 pixels is placed in the focal plane of the lens to implement the phase control between the horizontal and vertical components for different wavelength channels. One can modulate the polarization of the SHG pulses at different wavelengths by adjusting the corresponding phase of the diagram loaded on the SLM according to the spatial position of the spot. Then, the SH lasers are used to pump a CPPLN waveguide placed inside a polarization Sagnac loop to generate the polarization-entangled photon pairs. A dichroic mirror is leveraged to separate the photon pairs from the SHG pulses, and the entangled photon pairs are ultimately allocated to the end users by using an ITU DWDM filter. See Supplementary Section VI for further details about the central wavelength of the pump lasers and quantum channels. The photons distributed to all the end users are detected by SNSPDs with a detection efficiency varying from 60% to 80% and dark count rate of 40–100 counts per second. The photon detection results are recorded by a time-to-digital converter that is synchronized by the electric signal from the mode-locked fibre laser.

Data availability

All data are available in the article or its Supplementary Information. The data files supporting the plots in the main text are available via figshare at https://figshare.com/s/145209fe661ad4bcd80b (ref. 50). The data that support the findings of this study are available from the corresponding authors upon reasonable request. Source data are provided with this paper.

References

49. Zhang, Y. et al. Scalable, fiber-compatible lithium-niobate-on-insulator micro-waveguides for efficient nonlinear photonics. *Optica* **10**, 688–693 (2023).
50. Huang, Y. et al. SourceData.zip. *figshare* https://figshare.com/s/145209fe661ad4bcd80b (2025).

Acknowledgements

This work is supported in part by the National Natural Science Foundation of China (grant nos. 12192252 and 62375164), the Foundation for Shanghai Municipal Science and Technology Major Project (grant no. 2019SHZDZX01-ZX06), the Shuguang Program of Shanghai Education Development Foundation and Shanghai Municipal Education Commission (grant no. 24SG53), the National Key Research and Development Program of China (grant nos. 2022YFA1205100 and 2023YFA1407200), the Science and Technology Commission of Shanghai Municipality (grant no. 24JD1401700) and the Guangdong Provincial Quantum Science Strategic Initiative (grant no. GDZX2403003).

Author contributions

Y.H. and X.C. conceptualized the idea and designed the experiments. X.C. led the project since its conception. Y.L., Y. Zheng and X.C. supervised all the experiments. Y.H., Y.Y. and Z.Q. performed the experiment and data analysis. J.W., H.L., J.Q. and Y. Zhang developed the device fabrication. All authors participated in discussions of the results. Y.H. prepared the paper with assistance from all other co-authors. Y.Y., Y.L., Y. Zheng and X.C. provided revisions.

Competing interests

The authors declare no competing interests.

Additional information

Supplementary information The online version contains supplementary material available at https://doi.org/10.1038/s41566-025-01792-0.

Correspondence and requests for materials should be addressed to Yuanhua Li, Yuanlin Zheng or Xianfeng Chen.

Peer review information *Nature Photonics* thanks the anonymous reviewer(s) for their contribution to the peer review of this work.